IN-FLIGHT AND WIND TUNNEL LEADING-EDGE VORTEX STUDY ON THE F-106B AIRPLANE

John E. Lamar
NASA Langley Research Center
Hampton, Virginia

SUMMARY

The vapor-screen technique has been successfully applied to an F-106B fighter aircraft during subsonic and transonic maneuvers. This system has allowed the viewing of multiple vortex systems on the wing upper surface at angles of attack less than 19°. In addition, similarities as well as differences were determined to exist between the vortex systems for a full-scale semispan model and the flight vehicle at 20° incidence. Furthermore, variations in Reynolds number and Mach number have been identified as to how they affect vortex system details at flight conditions.

INTRODUCTION

The visualization of vortex systems which originate from aerodynamic surfaces is a common occurrence in wind tunnels, where techniques like tuft grids, schlieren, smoke wands, and vapor screens have been used (see refs. 1-6). Some of these seed the working fluid with smoke or sufficient water vapor (ref. 6) in order to highlight the core by either smoke entrainment or water condensation. This may occur along much of the length of the vortex, thereby yielding a visible record of the core path as can be seen in figure 1 for a wind tunnel model with upward deflected vortex flaps. Flight examples are not as readily available, but figure 2 shows the strake flow of an F-16 during a low-altitude maneuver. Both examples are the result of naturally occurring condensed water vapor (light areas) forming around and outlining the dark core regions.

In-flight use of smoke has been documented, in references 7 and 8, on delta wings to observe the leading-edge vortex breakdown progression (HP 115) and the outer panel flow (AVRO 707B) with increasing angle of attack, respectively. However, in order to obtain vortex system details, one needs to use a flight version of the vapor screen technique. Since the hardware to implement this was not available* when interest was expressed in observing the Reynolds number effects on the vortex system for the F-106B, the equipment had to be developed.** An illustration of what the vortex system looks like with such an implementation is shown schematically for the F-106B by the flight project logo in figure 3.

After the equipment was developed to seed the flow with vaporized propylene glycol in order that the observations be weather independent, illuminate the details with a light sheet, and record the events with a television system, applications were made

---

*Reference 9 reports the Soviet use of a ruby laser sheet and atmospheric water vapor to observe the vortex system at subsonic speeds above an ogee wing up to high incidence.

**Reference 10 used limited surface tufts near the middle of an F-106B wing during a flight test program and determined a reattachment line associated with a vortex system.

to both flight (see fig. 4) and wind tunnel vehicles. The particular information sought was to quantify the effect that the Reynolds number may have on the details of the leading-edge vortex system of full-scale vehicles at high angles of attack and subsonic speeds, including a 5-G transonic maneuver. This paper documents these results and offers a selected comparison of system details on a full-scale semispan F-106B model.

SYMBOLS

G	acceleration due to gravity, ft/sec^2
K	thousand
LE	leading edge
ι	inboard distance to vortex core from leading edge, inches
M	Mach number
m	inboard distance to inner edge of vortex system envelope from leading edge, inches
R_n	Reynolds number
TE	trailing edge
z	vertical distance to vortex core above upper surface, inches
α	angle of attack, degree

TEST SETUP

The wind tunnel tests were performed on a half-airplane model of the F-106B mounted in the Langley Research Center 30- by 60-Foot Wind Tunnel. This model was made by cutting an airplane in half and mounting it wingtip upward from a reflection plane. It should be pointed out that the full-scale model differed primarily from the flight vehicle only in the leading-edge region. The former had all the camber, essentially conical, ahead of the local 90-percent semispan; whereas, the latter had its conic-like camber ahead of the 80-percent local semispan. They are called Case XIV and Case XXIX cambers, respectively, by the manufacturer.

The tests in the 30- by 60-Foot Wind Tunnel were for the purpose of establishing starting values for the flight project in the areas of seeding flow rate and probe position, light-sheet width and orientation, and TV camera parameters. One great uncertainty remained after the wind tunnel test, and it was whether sufficient seeding material could be produced to make the vortex system visible at flight speeds.

The range of test parameters for the wind tunnel and flight is given in figure 5. This range includes the vapor screen variables such as seeding flow rate and probe position, and light-sheet width and location, as well as the two different types of maneuvers flown. The wind tunnel conditions are standard ones with the dynamic pressure not exceeding 10 lb/ft^2.

For both the 1-G constant altitude and the 5-G transonic maneuvers, six probe positions were tried in order to find the one that worked best overall. Five of these were underneath the leading edge and one was on top. These positions were numbered sequentially, and number 6 was found to be preferable. Its approximate location underneath the leading edge is shown on figure 6, along with the relative locations of the camera and light sheet.

The right side of this figure shows the view displayed on the monitor. Since the camera is looking down and aft onto the left wing panel, the wing trailing edge is at the top of the screen, the leading edge intersects the right side, and the fuselage cuts across the left corner. The light sheet is seen to lie in the middle of the screen and does not extend to the wing leading edge because of camber.

There were two light sheet locations used in the wind tunnel, one perpendicular to the fuselage centerline and the other perpendicular to the wing leading edge, as can be seen in figure 7. For the flight experiment, it was the intent to have the light also perpendicular to the leading edge. However, space constraints associated with attaching the light source to the fuselage limited the sheet to only reaching 11° ahead of perpendicular to the centerline as opposed to the 30° desired for this 60° swept wing. Hence, the light sheet location used in flight is closer to the more aft one used in the wind tunnel.

The slit width in the light sheet generator was varied from 0.003" to 0.041" for both wind tunnel and flight with most testing done at 0.041". In addition, most of the seeding was done with the pump operating at approximately 3 gallons per hour. For both of these systems, the intent was to use the smallest amount possible which would still seed and illuminate the vortex system sufficiently.

RESULTS AND DISCUSSION

It should be remembered that the primary data taken, other than test conditions, during both the flight and wind tunnel tests are video-tape visual records of the vortex systems. Using these records, photographs of portions of particular flights were made from a monitor in order that a comparative study may be done and the pertinent test effects may be identified. (The photographs presented are from an orientation delineated on the right-hand side of figure 6.)

From flight, there are basically two kinds of effects to be presented corresponding to the two types of flights flown. The first type is one in which the altitude is held essentially constant, and the Mach number is adjusted to keep the aircraft at 1-G flight over an angle-of-attack range up to 23°. For each of these constant altitude flights, which ranged from 35,000 feet to 15,000 feet in 5,000-feet increments, the Mach number did not vary appreciably from 0.4; however, the Reynolds number increased by 6×10^6 as the altitude decreased. The other type was for a transonic maneuver at 5-G and $M \sim 0.8$, accomplished during a spiral descent, at a fixed angle of attack, 19°, in which the Reynolds number varied significantly.

Effect of Reynolds Number

The effect of Reynolds number can be seen in figures 8 to 13, using comparative photographs at angles of attack from 17° to 23°. These 1-G flights show that at 17°, leading-edge separation is well established at $R_n = 26 \times 10^6$, which corresponds to the highest altitude, but has not even begun at $R_n = 32 \times 10^6$. Between these extremes, progressively smaller amounts of leading-edge separation are noted with increasing Reynolds number. Much the same occurs at 18°, but at 19° there is a first indication of leading-edge separation at the highest Reynolds number. The delay in separation onset associated with increasing Reynolds number is not new for round-edged wings with camber, but that it would be observed in flight is remarkable.

It is also noteworthy to point out evidences of other vortical action inboard of the leading edge at $\alpha = 19°$ and $R_n = 32 \times 10^6$. The innermost may be associated with the juncture flow; however, the mid-semispan vortex may well be coming from the upper surface shear layer tearing and forming another system of the same rotational sense as at the leading edge. This may occur when the leading-edge vortex is not yet strong enough to dominate the entire outer panel flow. Figure 11 has been prepared to show the postulated positions of the various vortical systems at the 20,000-feet altitude. When this system is viewed from above, it has an appearance which resembles the discrete vortices in the feeding sheet, arranged roughly parallel to the leading edge, around the primary vortex found in water tunnel tests and reported in reference 11. One important difference is that, in flight, each vortex extends to the upper surface.

Figure 12 shows that, at 20°, only a single vortex system exists outboard and, as it gets bigger with decreasing Reynolds number, the innermost one grows smaller. The same is true at 23°, as seen in figure 13.

It is apparent from this series of comparative photographs that the leading-edge vortex is Reynolds number dependent. To help establish the quantitative dependence, figure 14 has been prepared in which the vortex system envelopes and "cores" have been determined for two different values of Reynolds number. They are displayed against the aft part of the left wing panel and are for values of angle of attack from 18° to 23°. The "cores" are not determined from finding the "black hole," since none was seen for these flights, but are established by an examination of where the smoke was the brightest and its rotation centered. The brightest smoke was chosen since it represented an increased density/reflectivity which one would expect to surround the very core itself. By superimposing the results shown in figure 14 onto a similarly recorded target board marked off in 6-inch squares, quantifiable information was established for the inner extent of the envelope and core location; this information is presented in figure 15.

From this figure it can be seen that, in general, the inner extent of the vortex system envelope and of the core locations is more inboard at the lower Reynolds number. Also, at the lower value, the envelope and core tend to be more monotonic in their growth with angle of attack. It is interesting to note that at 20° the results seem to coalesce, after which the measurements corresponding to the higher Reynolds number have a slower inboard growth. The core elevation seems insensitive to Reynolds number.

Figure 16 compares these results, taken from the Case XXIX flight wing, with those from the 30- by 60-Foot Wind Tunnel test of the Case XIV wing. Though the vortex flow was much unsteadier in the wind tunnel, as its lateral position oscillated between outboard and inboard, an interpolated aggregate position, shown by the filled diamond, does compare surprisingly well with the flight data. The interpolation is required since the light sheet locations used in the wind tunnel lie on either side of the flight position. Note that the height of the wind tunnel core is above the flight ones. No other conclusions can be drawn, since there was not enough time in the wind tunnel with the right probe position to get sufficient data.

Effect of Mach Number

Figure 17 provides details of the vortex systems for both 1-G and 5-G flights, which occurred at roughly 0.4 and 0.8 Mach number, respectively. These photographs were taken with two different light sheet widths, and the 5-G maneuvers were done both to

the left and right to rule out any centrifugal force effects on the results. Basically, with either light sheet width, the vortex appears similar under these test conditions. However, for the thinner light sheet and 5-G maneuver, one is able to see a core along with what appears to be a shear layer feeding into it.

To identify the effect of Mach number, the envelope and core are compared in figure 18 for these two different maneuvers. It is readily apparent that the doubling of Reynolds number has not delayed the leading-edge vortex formation to a higher angle of attack. This is in contrast to the effect of increasing Reynolds number discussed previously (see fig. 10). The more inboard extent of the envelope and of the core is therefore attributed to the Mach number doubling. This was an unexpected effect.

CONCLUDING REMARKS

In this paper, two basic topics have been covered: vapor screen technology implementation for manned flight vehicles, in particular, the F-106B, and the vortex system features revealed by using this technology in flight and in the wind tunnel. Regarding the first topic, it has been demonstrated that the vapor screen technique can be applied successfully to large-scale vehicles both in the wind tunnel and in flight under a variety of test conditions. These include the transonic maneuver, which future fighter aircraft will continue to need to perform.

Concerning the results obtained using this technique, significant differences have been noted in the size of the leading-edge vortex system and its core location at subsonic speeds with only relatively small changes in flight Reynolds number. The prime effect seems to be the well-known delay of separation on round-edged wings associated with increased Reynolds number. At 20° angle of attack, where flight and wind tunnel vortex system details could be directly compared, there was close overall agreement even with differences in wing camber and with the flight Reynolds number being greater by a factor of 2. This occurred in spite of the vortex system being more stable in flight than in the wind tunnel. In addition, during the transonic maneuver, the Mach number effect can overcome the trend of increasing Reynolds number to reduce the vortex system by producing a larger, more inboard, and well-defined vortex system relative to the constant altitude 1-G flight.

REFERENCES

1. Settles, G. S.: Flow Visualization Techniques for Practical Aerodynamic Testing. Presented at the Supersonic Tunnel Association Meeting, Williamsburg, Virginia, October 1983.

2. Peake, D. J.; and Tobak, M.: On Issues Concerning Flow Separation and Vortical Flows in Three Dimensions. Aerodynamics of Vortical Type Flows in Three Dimensions, AGARD CP-342, Paper No. 1, 1983.

3. Werlé, H.: Visualization des Ecoulements Tourbillonnaires Tridemensionnels. Aerodynamics of Vortical Type Flows in Three Dimensions, AGARD CP-342, Paper No. 8, 1983.

4. Wentz, W. H., Jr.: and Kohlman, D. L.: Wind-Tunnel Investigation of Vortex Breakdown on Slender Sharp-Edged Wings. NASA CR-98737, 1968.

5. Snow, W. L.; and Morris, O. A.: Investigation of Light Source and Scattering Medium Related to Vapor-Screen Flow Visualization in a Supersonic Wind Tunnel. NASA TM-86290, December 1984.

6. Jorgensen, L. H.: Prediction of Static Aerodynamic Characteristics for Slender Bodies Alone and with Lifting Surfaces to Very High Angles of Attack. NASA TR R-474, September 1977.

7. Fennell, L. J.: Vortex Breakdown - Some Observations in Flight on the HP 115 Aircraft. R&M No. 3805, British A. R. C., 1977.

8. Perry, D. H.; Port, W. G. A.; and Morrall, J. C.: Low Speed Flight Tests on a Tailless Delta Wing Aircraft (AVRO 707B). C.P. No. 1107, British A. R. C., 1970.

9. Burdin, I. Yu.; Zhirnov, A. V.; Kulesh, V. P.; Orlov, A. A.; Pesetskiy, V. A.; and Fonov, S. D.: Use of Laser Methods for the Study of Detached Flows in a Wind Tunnel and in Flight. Translated from "Scientific Notes of TsAGI-Central Institute of Aerohydrodynamics," USSR, 1981, pp. 1-19.

10. Chamberlin, R.: Flight Investigation of 24° Boattail Nozzle Drag at Varying Subsonic Flight Conditions. NASA TM X-2626, November 1972.

11. Gad-el-Hak, M.; and Blackwelder, R. F.: The Discrete Vortices from a Delta Wing. AIAA Journal, Vol. 23, No. 6, June 1985, pp. 961 and 962.

BIBLIOGRAPHY

Other useful papers dealing with in-flight flow visualization are listed below for completeness.

1. Roberts, S. C.; and Smith, M. R.: Flow-Visualization Techniques Used in Full-Scale Flight Tests. TRECOM Technical Report 64-39, U. S. Army Transportation Research Command, Ft. Eustis, VA., July 1964.

2. Curry, R.; Meyer, R. R., Jr.; and O'Connor, M.: The Use of Oil for In-Flight Flow Visualization. NASA TM-84915, August 1983.

Subsonic
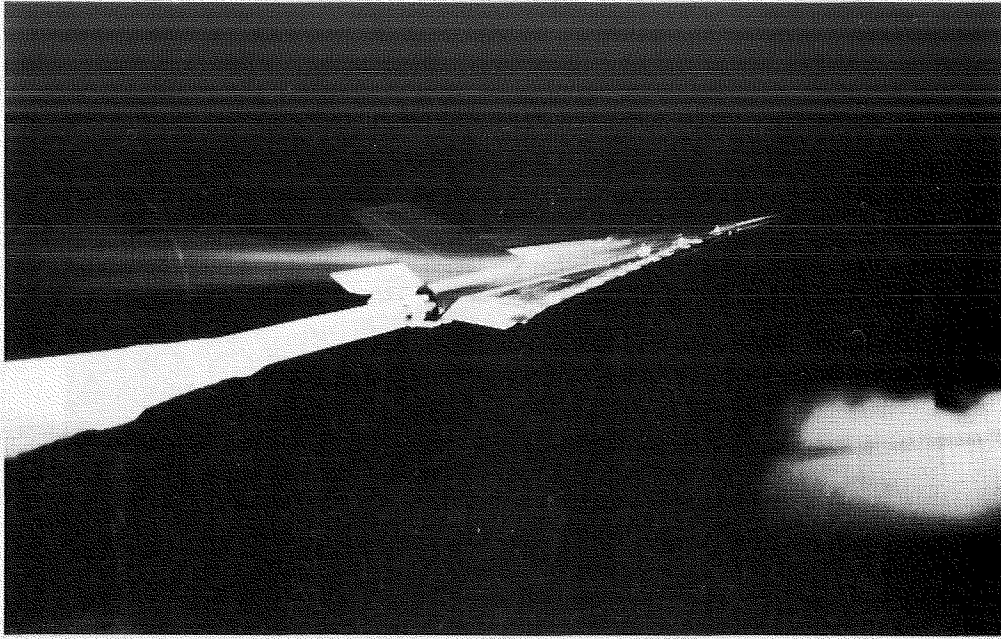
Figure 1. Leading-edge vortex core visualization on 74° delta with upward deflected vortex flap.
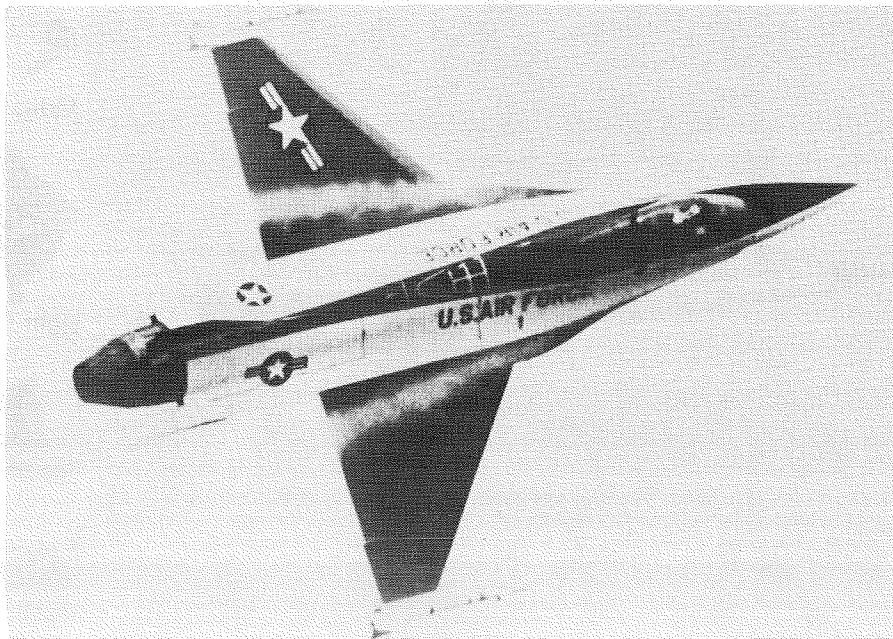
Figure 2. Strake vortex core visualization on F-16 during low-speed maneuver.

Figure 3. Flight project logo.

Video Camera

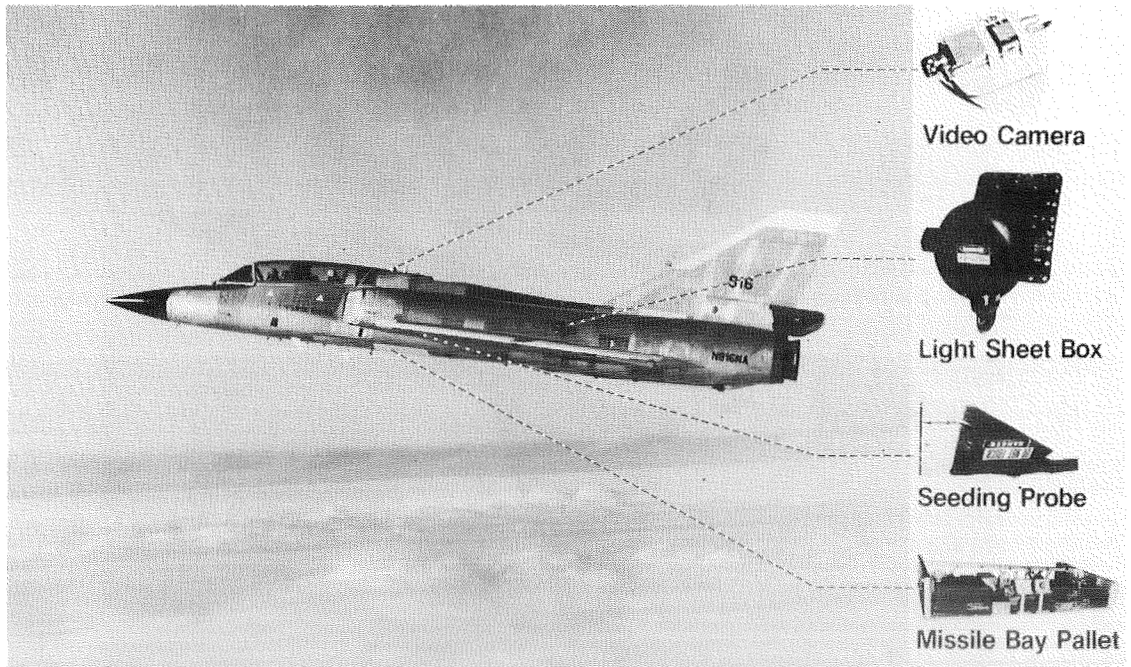Light Sheet Box

Seeding Probe

Missile Bay Pallet

Figure 4. F-106 flow visualization elements.

- Vapor screen variables
  - Seeding flow rate - (1. 5 ⟶ 3. 6 gal/hr)   3. 0 gal/hr
  - Probe position - 6 tried in flight , # 6 preferred
    - many tried in wind tunnel, one preferred
  - Light slit/sheet width - (.041", .012", .003") .041"
  - Light sheet location - one in flight
    - two in wind tunnel
- Flight conditions
  - Constant altitude 1-G decelerations -(35K, 30K, 25K, 20K, 15K, ft)
    M ~ .4,   α ≤ 23°
  - Spiral descent ~5 G, 40K, ft ⟶20K, ft (right and left)
    M ~ .8,   α ~ 19°
- Wind tunnel conditions
  - Mach number   ≤ .10
  - Angle of attack,   12° ⟶ 20°
  - Elevon deflection,   15° down ⟶27° up

Figure 5.   Test parameters.
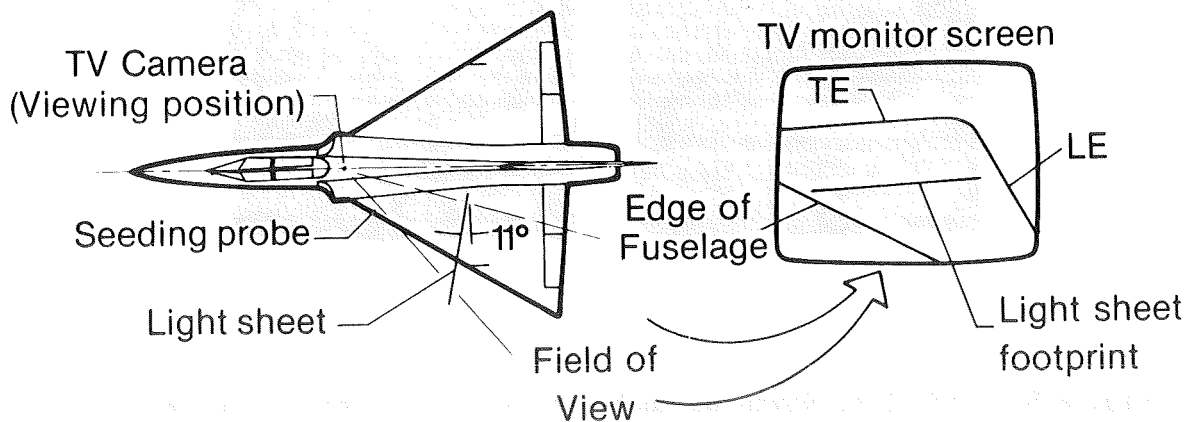
Figure 6.   In-flight leading-edge vortex flow visualization on F-106B.
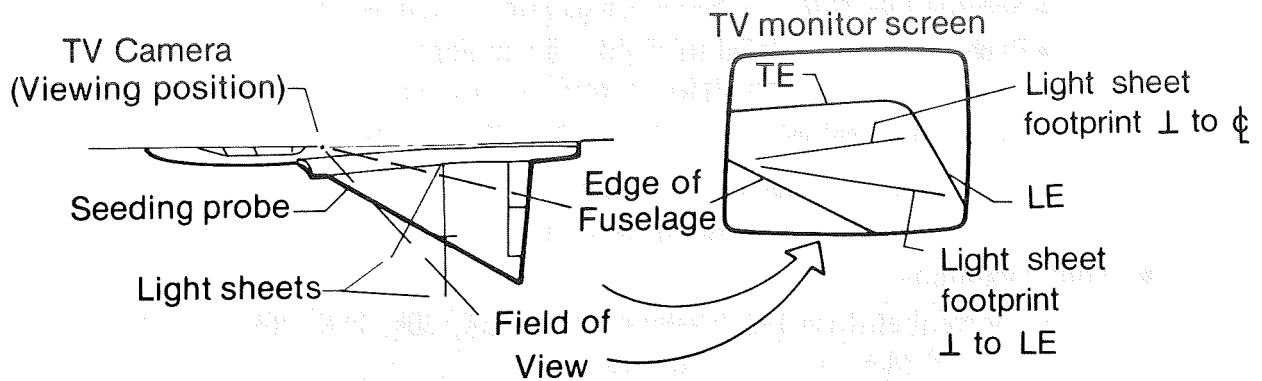
Figure 7 - Wind tunnel (30- by 60-ft) leading-edge vortex flow visualization on F-106B.
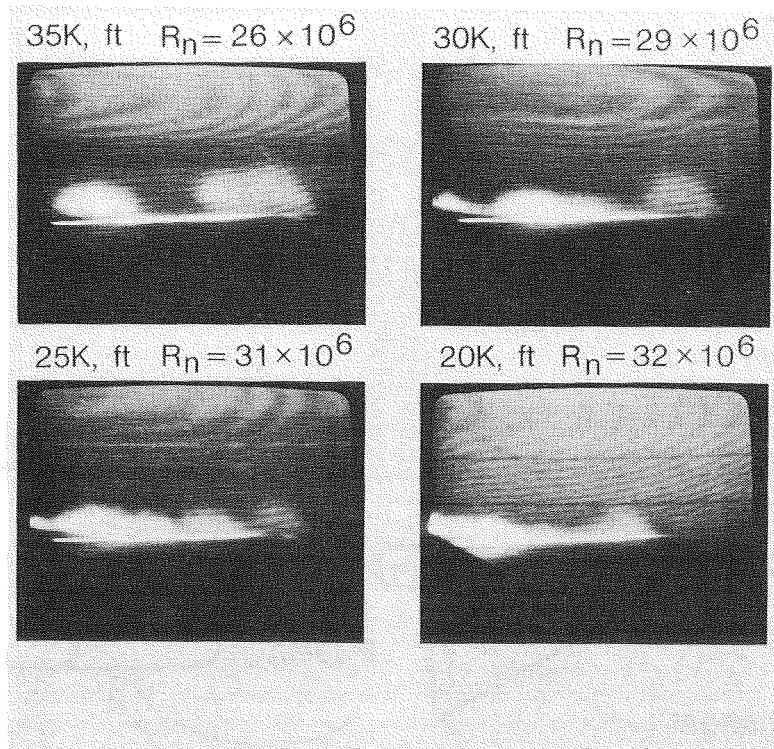
Figure 8. Effect of Reynolds number on vortex system, ~ 1G, probe #6, slit width = .041 in., $\alpha \sim 17^0$.

196
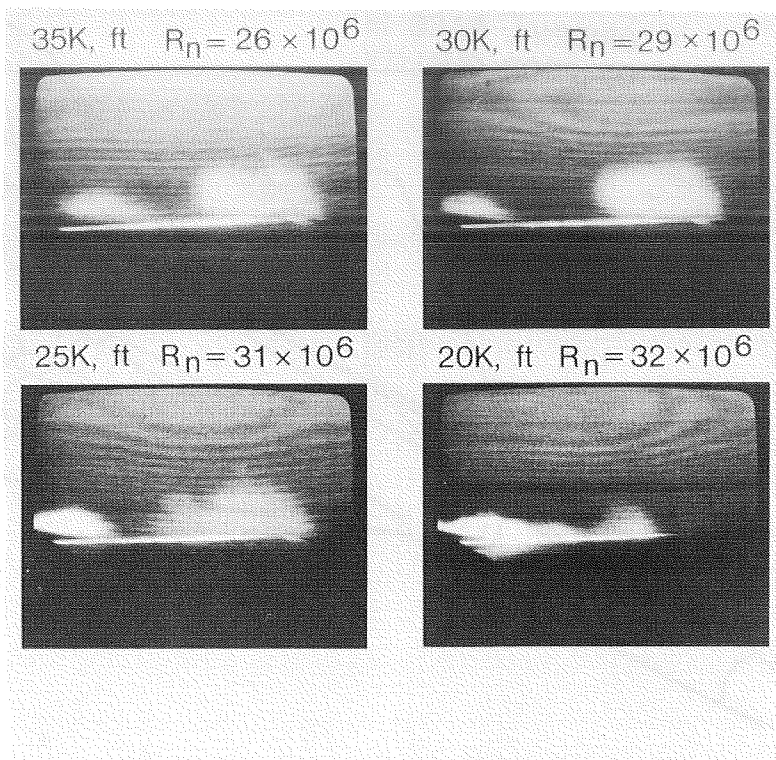
Figure 9. Effect of Reynolds number on vortex system, ~ 1G, probe #6, slit width = .041 in., $\alpha \sim 18^0$.
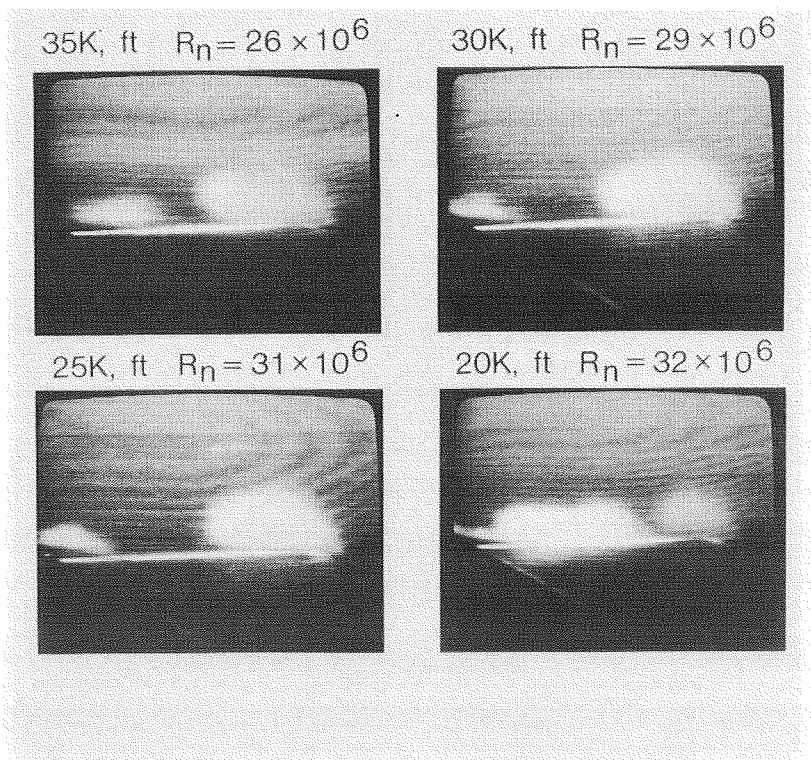
Figure 10. Effect of Reynolds number on vortex system, ~ 1G, probe #6, slit width = .041 in., $\alpha \sim 19^0$.
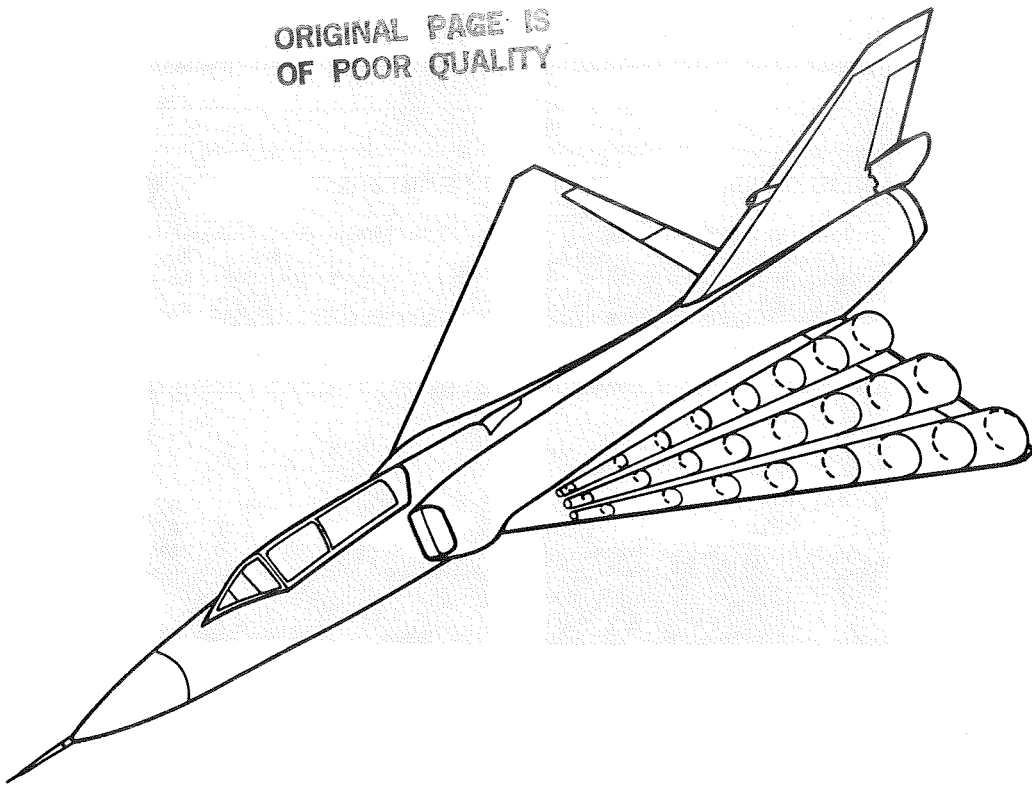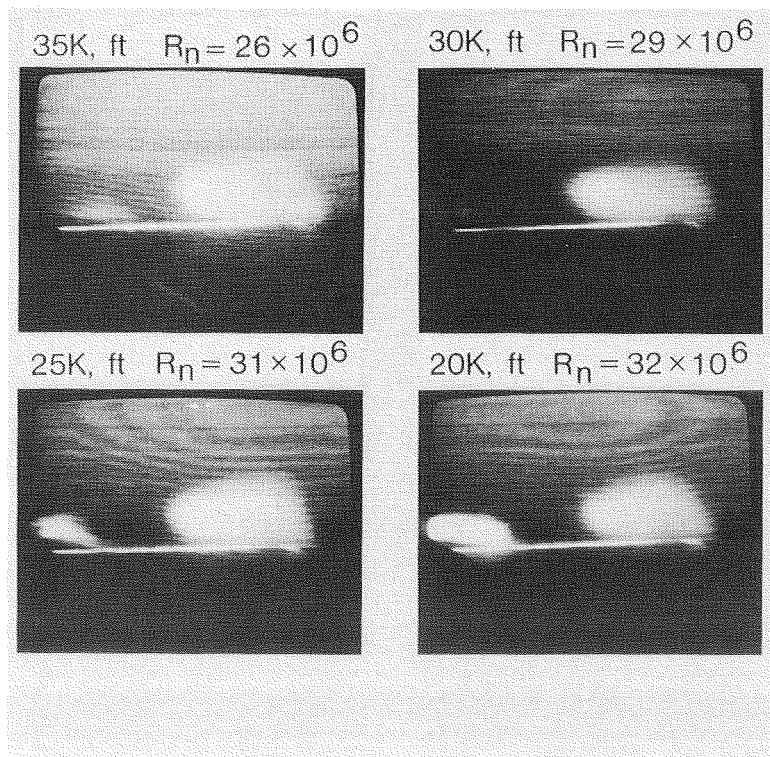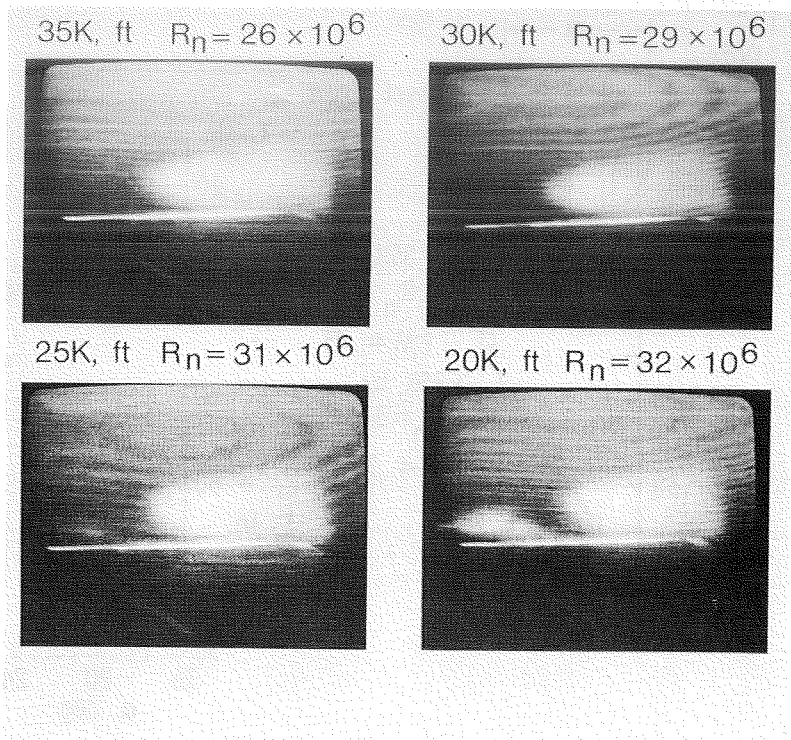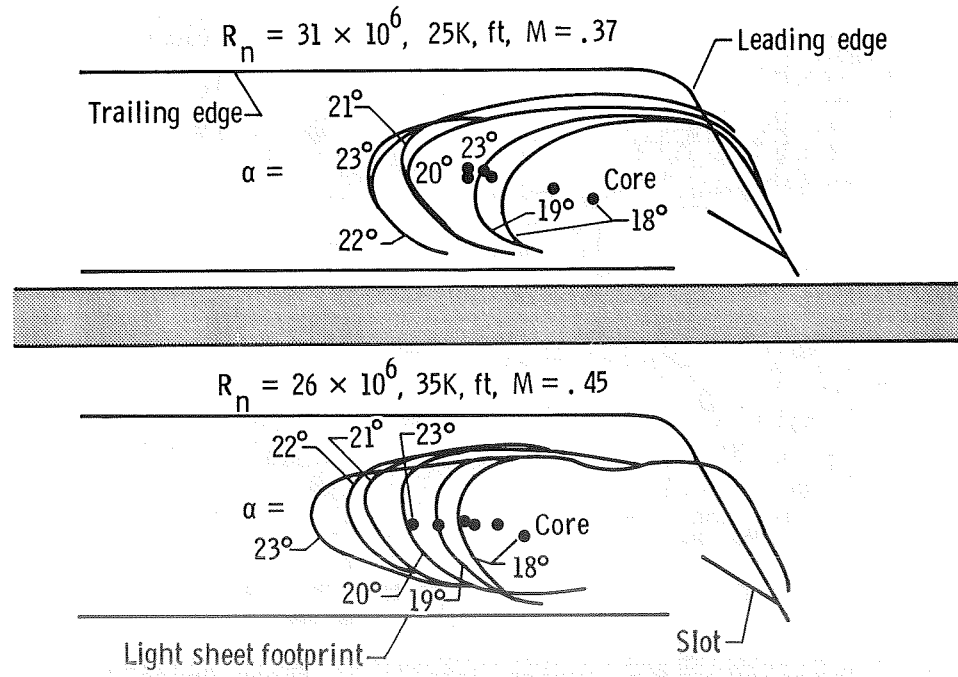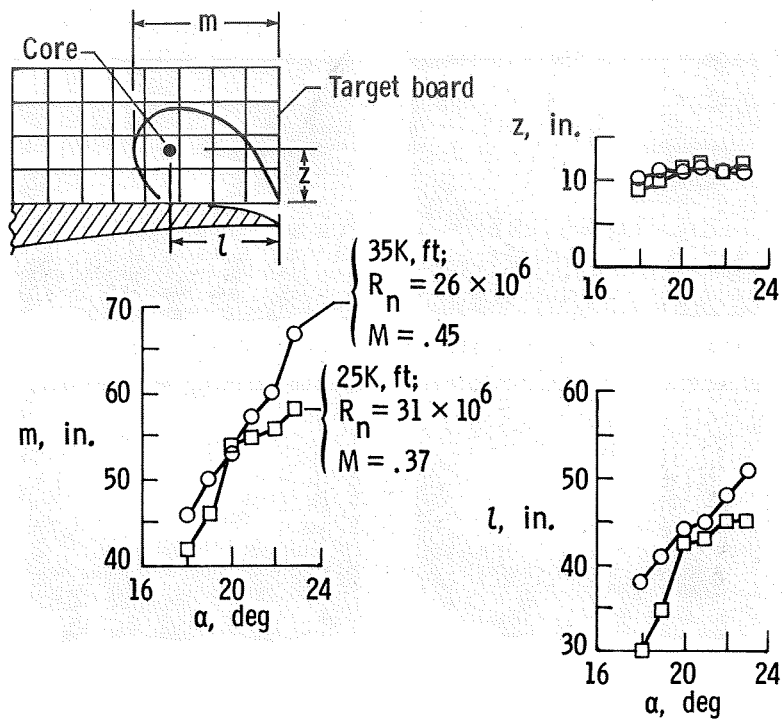
Figure 11. Multiple vortex systems on round-edged cambered delta, $\alpha \leqslant 19^0$, 1G.

Figure 12. Effect of Reynolds number on vortex system, $\sim$1G, probe #6, slit width = .041 in., $\alpha \sim 20^0$.

Figure 13. Effect of Reynolds number on vortex system, ~ 1G, probe #6, slit width = .041 in., $\alpha \sim 23^0$.

Figure 14. Effect of Reynolds number on vortex system, 1G, probe #6.

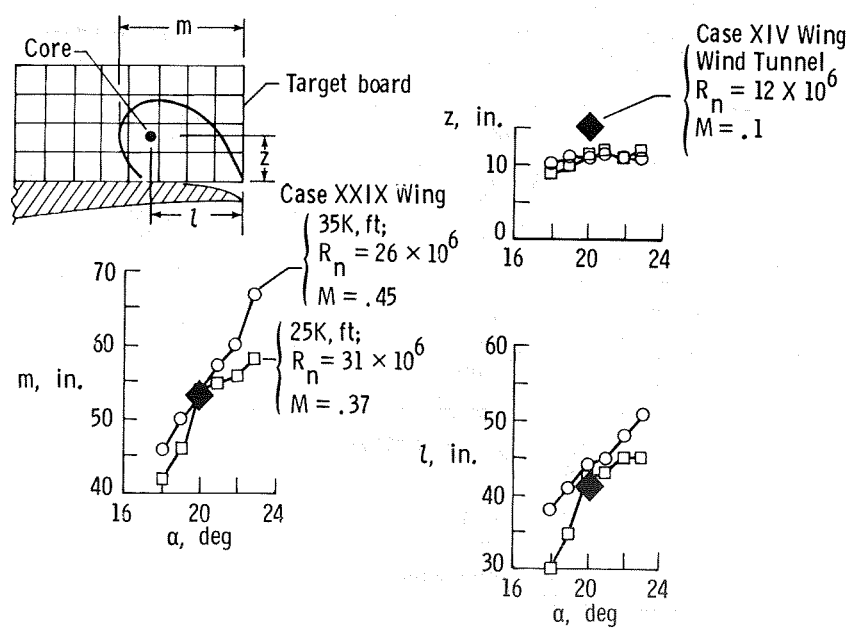Figure 15. Measured vortex system details at two Reynolds numbers, 1G, probe #6.

Figure 16. Measured vortex system details at three Reynolds numbers, 1G, probe #6.
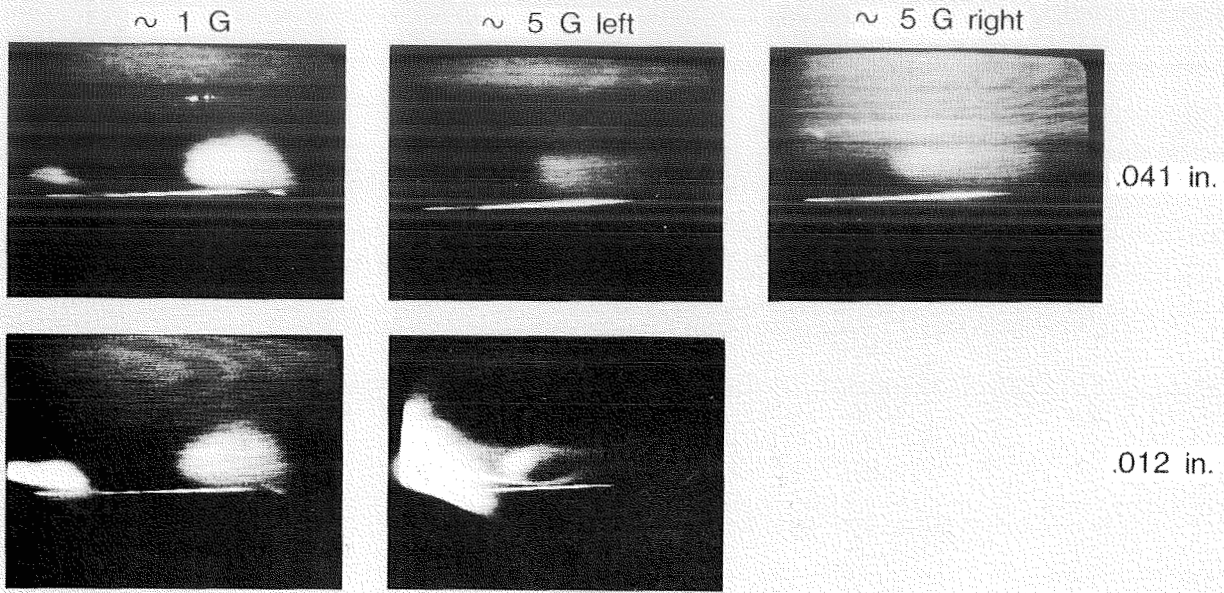
Figure 17. Vortex system details at two maneuvers and slit widths,
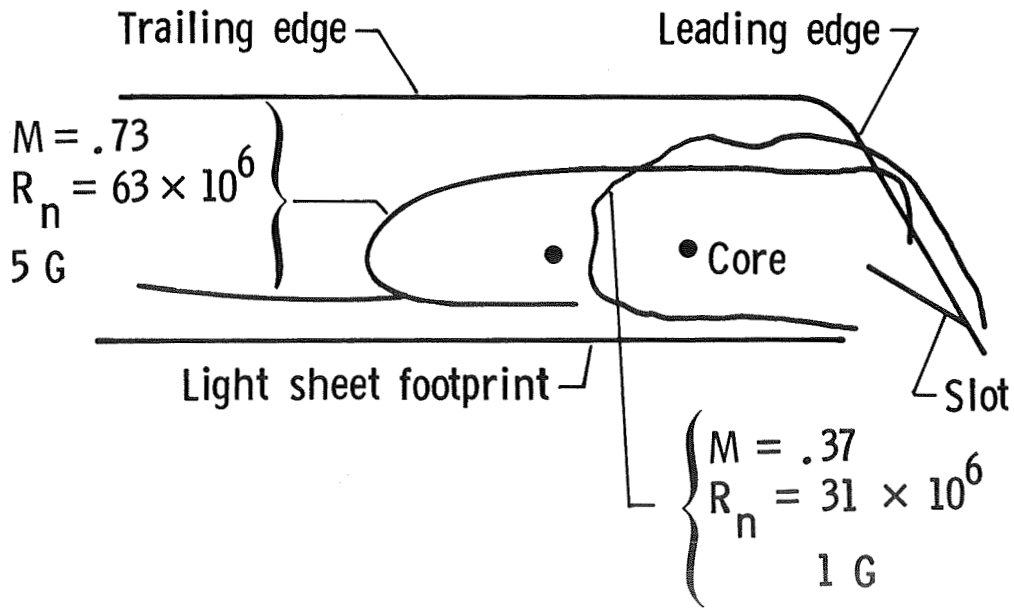$\alpha \sim 19^0$, $\sim$ 25K ft, probe #6.

Figure 18. Effect of Mach number and load factor on vortex system,
$\alpha = 19^0$, 25K ft.